sciendo
Power Electronics and Drives
Volume 9(44), 2024 DOI: 10.2478/pead-2024-0023

Magnetic Decoupling: Basis to Form New Electrical Machines

Research paper

Yalla Tirumala Rao[1,*], Chandan Chakraborty[2]

[1]*Software Department, Danfoss Industries Pvt. Ltd., Chennai, India*
[2]*Department of Electrical Engineering, Indian Institute of Technology, Kharagpur, India*

Received: 27 March 2024; Accepted: 24 May 2024

Abstract: Magnetic decoupling principle when applied to electrical machines states that if two windings are configured for different number of pole pairs, they would not interact with each other magnetically even though they share a common magnetic core. This principle forms the basis for developing special machines where two or more machines can be integrated with the same magnetic circuit. This paper deals with formulating the mathematical analysis that determines the validity of this principle during practical conditions (i.e. non-sinusoidal winding distribution, flux saturation, etc.). Extensive Finite Element Method (FEM) simulation results from the Ansys Maxwell-2D software platform closely obey the conclusions derived from the mathematical analysis. As an example, new brushless and magnetless synchronous machines (SMs) have been developed by using this principle. It is designed by embedding an induction machine (IM) with a SM. Experimental investigations conducted on the laboratory prototype support the mathematical analysis dealt with in this paper.

Keywords: *brushless synchronous generator • induction machine • magnetic decoupling principle • synchronous machine*

1. Introduction

Multi-winding machines are currently gaining attention from researchers in the field of electrical machines due to their high reliability, higher power density and inherent fault tolerance. Most of the machines are targeted for high-power applications like rolling mill drives (Dhaouadi et al., 1993), ship propulsion systems, wind energy conversion systems (Ademi et al., 2015), etc. Also, safety is a major concern for these systems. Therefore, such systems avoid the deployment of brushes and slip rings to render them rugged and maintenance-free. Different winding connections have been investigated in the literature to make the system brushless. In some cases, the magnetic coupling between the windings has been utilised to form an alternative for the doubly-fed induction generators (as done for dual-stator-winding induction generators [Liu *et al*., 2024]). In such cases, the pole configuration of both the windings are same. However, in most cases, magnetic decoupling between the windings is preferred to integrate multiple windings in the same machine frame (Cingoski et al., 1999; Vaidyaa et al., 1998).

One such example can be a brushless doubly fed induction machine (IM) (Ademi et al., 2015). This machine consists of two stator windings wound for different pole pairs. Even though these two windings are magnetically decoupled, the rotor couples them electrically through a nested-loop structure. Dual stator winding IMs of different pole combinations have also been reported in Guerrero and Ojo (2009) and Munoz and Lipo (2000). In this case, the merits of a 2/6 pole (with a ratio of 1:3) combination (Guerrero and Ojo, 2009) have been highlighted (e.g. better core utilisation). However, such benefits can be attained only if both windings are independently controlled through power electronic converters. In Vaidyaa et al. (1998), two synchronous machines (SMs) were embedded by sharing the same core but configured for different number of poles to generate different frequency output voltages.

Traditional brushless synchronous generators necessitate the use of a separate exciter machine (Griffo et al., 2013). Such machines consume additional space/floor area and so the integration of these two machines has become an area of active research. Self-excited brushless synchronous generators (Inoue et al., 1992; Nonaka and Kawaguchi, 1992) have been proposed in the early 90s where the space harmonics will be collected by a harmonic

* *Email: yallatirumala@gmail.com*

winding placed on the rotor. A rectified induced voltage of the harmonic winding will be used to feed the field winding of the SM (Inoue et al., 1992). Though these systems are simple in structure, control on the excitation is not available. To have a control on the amplitude of the space harmonics (therefore the excitation), various harmonic excitation schemes have evolved to develop brushless wound-field synchronous generators. One such scheme has been reported where a third harmonic is deliberately injected into the open-ended stator windings using two controlled converters (Yao et al., 2015, 2021). The injected harmonics create a static magnetic field that couples only with the harmonic winding (placed on the rotor) and feeds the main field winding through a rotating rectifier. To simplify the controller, an additional harmonic winding (Yao et al., 2016) has been incorporated into the stator such that this winding does not interact with the magnetic field corresponding to the main machine. In Ali et al. (2015), Hussain and Kwon (2018), Rafin and Mohammed (2023) and Ayub et al. (2019), different kinds of harmonics-based brushless synchronous generators are proposed. In that, some of them use two inverters (Ali et al., 2015; Rafin and Mohammed, 2023) at the stator side, and the other has a special stator winding distribution (Hussain and Kwon, 2018) for developing the harmonics in the air gap. In Jawad et al. (2016), Yao et al. (2022) and Hammad et al. (2023), zero/third harmonic are developed due to the power electronics at the stator winding (for example in Jawad et al. (2016) and back-to-back thyristors in parallel to each phase of the stator winding) are used to develop zero sequence/third harmonic in the space.

Even though magnetic decoupling between the windings forms the basis for the fabrication of above-mentioned machines, a detailed analysis of the magnetic interaction between the windings of different pole configurations has not been reported in the literature. This work deals with the development of a mathematical analysis which indicates the suitability of pole combination to accomplish magnetic decoupling considering practical situations. Section 2 deals with the mathematical framework of the magnetic decoupling principle by considering sinusoidal winding distribution. An extension of this principle for practical situations has been reported in Section 3. By using this principle a new brushless and magnet-less SM is developed. The basic system structure and principle of operation of this machine are discussed in Section 4. Maxwell-2D-based simulation to verify the above analytical study is presented in Section 5. Prototypes of the proposed machine have been developed and experimental results corresponding to the magnetic decoupling nature are presented in Section 6. Section 7 concludes the work.

2. Magnetic Decoupling Theory

The magnetic decoupling principle states that, in any machine, if two windings are configured for different number of poles, they do not influence each other magnetically even though they are present in the same core (Chakraborty and Rao, 2019). However, certain ideal conditions must be met to achieve the perfect magnetic decoupling between the windings which are as follows.

a. All windings of the machine should be distributed in a sinusoidal manner.
b. B-H characteristics of the core material should be linear. On the other sense, saturation of the BH curve of the core material is neglected.
c. Space harmonics in the magnetic field due to the slot openings should be zero.

This phenomenon can be explained by considering a fictitious machine that consists of *q*-pole, *m*-phase distributed winding on the stator and *p*-pole concentric winding on the rotor as illustrated in Figure 1a. To understand the magnetic decoupling nature between the windings, the rotor of the fictitious machine (see Figure 1a) is excited with i_r current, and flux linked by the stator windings due to this rotor current is analysed in this work. Note that excitation provided to the stator windings of the fictitious machine is zero in this case. Flux linking (Krause et al., 2013, p. 50) with all phases of the stator winding when only the *p*-pole rotor winding is excited are demonstrated as

$$\psi_{qspr}(m_x)=\sum_{n=0}^{\frac{q}{2}-1}(-1)^n\int_{\frac{2\pi n}{q}}^{\frac{2\pi(n+1)}{q}}\mathbb{N}_{ms}\int_{\phi_s+\frac{2(n-1)\pi}{q}}^{\phi_s+\frac{2n\pi}{q}}B_r(\zeta,\theta_r)\alpha rld\zeta d\phi_s=\frac{-4g}{p}\sin\left(\frac{\pi p}{q}\right)\sum_{n=0}^{\frac{q}{2}-1}\left\{\begin{array}{l}\dfrac{\sin\left(\dfrac{p\theta_r}{2}+\dfrac{2\pi(m_x-1)}{m}-\dfrac{2pn\pi}{q}\right)}{p+q}\\+\dfrac{\sin\left(\dfrac{p\theta_r}{2}-\dfrac{2\pi(m_x-1)}{m}-\dfrac{2pn\pi}{q}\right)}{q-p}\end{array}\right\}=0 \quad (1)$$

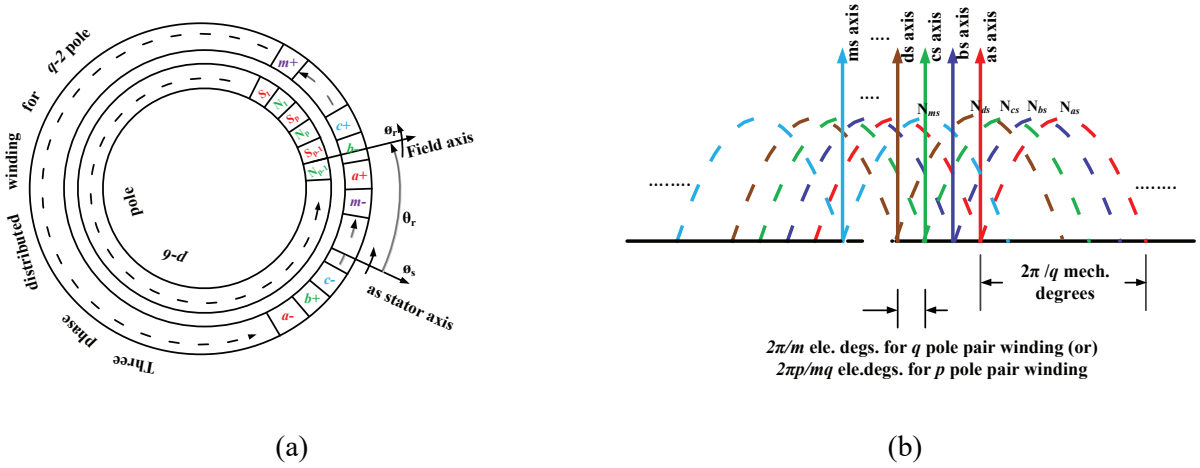

(a) (b)

Figure 1. (a) A fictitious machine with *q*-pole, *m*-phase winding on the stator and *p*-pole winding on the rotor. (b) Sinusoidal distribution of *q*-pole *m*-phase stator winding of fictitious machine.

Here, $g = \frac{N_s\ N_r\ \mu_0\ i_r\ \alpha\ r\ l}{pq}$ and $\mathbb{N}_{ms} = \frac{N_s}{q}\sin\left(\frac{q\phi_s}{2} - \frac{2\pi(m_x - 1)}{m}\right)$ is the winding distribution function of the *q*-pole, *m*-phase stator winding. m_x is 1, 2, 3 … *m* for phase-*A*, phase-*B*, phase-*C* … phase-*m*, respectively. Note that all these windings are sinusoidally distributed as demonstrated in Figure 1b. Similarly, $B_r = \frac{\mu_0 N_r I_r}{p}\sin\left(\frac{p\zeta - p\theta_r}{2}\right)$ is the air-gap flux densities developed by the *p*-pole rotor winding of the fictitious machine. As discussed earlier, space harmonics developed due to the slot openings are neglected. As it is known, there are $\frac{q}{2}$ parallel paths (*q*-pole stator winding of the fictitious machine) can be possible. Each term in Eq. (1), represents the flux linked by each parallel path of the *q*-pole stator winding of the fictitious machine. From the above analysis, individual coils of the *q*-pole stator windings may have non-zero flux linkage. Nevertheless, the vector sum of all these coils flux-linkages corresponding to that phase will cancel themselves while forming a *q*-pole winding. Therefore, flux-linked by *q*-pole winding due to the excitation provided to the *p*-pole rotor winding is zero when *p* is not equal to *q*. This means the energy converted from mechanical to electrical form or electrical to mechanical form is zero. However, in practice, these winding functions may not be distributed sinusoidally due to the limited number of slots. Apart from that, flux developed by *p*-pole rotor winding might have space harmonics due to the slot openings and core saturation. A detailed analysis of these practical situations is explained in the following section.

3. Analytical Study Considering Non-idealities

As discussed before, non-idealities in constructing a machine due to practical challenges will influence the magnetic decoupling nature between the stator and rotor windings of the fictitious machine as shown in Figure 1. The following sub-sections discuss elaborately the effect of these non-idealities.

3.1. Non-sinusoidal winding distribution

In general, the winding function of the practical machine is not pure sinusoidal due to the limited number of slots. The winding function of a fractional pitched and uniformly distributed winding can be illustrated as shown in Figure 2. In this case, the winding distribution function of the stator windings of the fictitious machine can be expressed as (Lipo, 2012, p. 22):

$$\mathbb{N}_{ms} = \frac{2N_s}{\pi q}\sum_{h=1,3,5}^{\infty}\frac{k_{wh}\sin\left(h\left(\frac{q\phi_s}{2} - \frac{2\pi(m_x - 1)}{m}\right)\right)}{h} \quad (2)$$

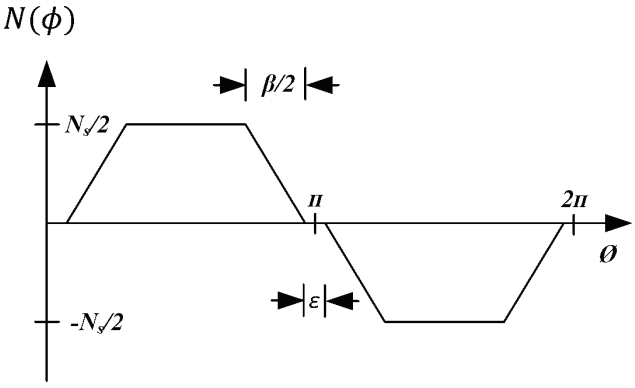

Figure 2. Fractional pitch, uniformly distributed winding distribution function (Lipo, 2012).

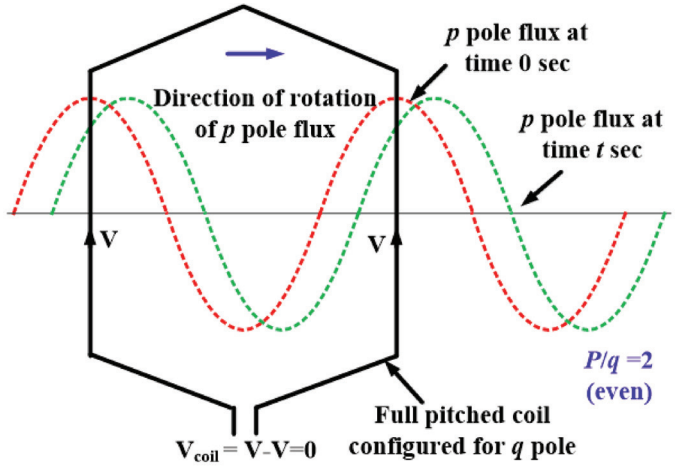

Figure 3. Effect of p pole flux on the full-pitched coil configured for q pole when p/q is equal to 2 ($p = 4$ and $q = 2$).

Here, $k_{wh} = \dfrac{\sin\left(\frac{h\beta}{4}\right)}{\frac{h\beta}{4}} cos\left[h\left(\frac{\beta}{4}+\frac{\varepsilon}{2}\right)\right]$ is the harmonic winding factor of short pitched, uniformly distributed windings as illustrated in Figure 2. ε and β are short pitch angle and distribution angles, respectively. Considering the non-sinusoidal winding distribution, flux-linking with stator windings of the fictitious machine, when the p-pole rotor winding is excited can be obtained by inserting Eq. (2) in Eq. (1) as follows.

$$\psi_{qspr}(m) = \frac{-4g}{p}\sum_{h=1,3,5}^{\infty}\frac{k_{wh}}{h}\sin\left(\frac{\pi p}{q}\right)\sum_{n=0}^{\frac{q}{2}-1}\left\{\frac{\sin\left(\frac{p\theta_r}{2}+\frac{2\pi(m_x-1)h}{m}-\frac{2pn\pi}{q}\right)}{p+hq}+\frac{\sin\left(\frac{p\theta_r}{2}-\frac{2\pi(m_x-1)h}{m}-\frac{2pn\pi}{q}\right)}{hq-p}\right\} \quad (3)$$

It could be possible to select the number of poles such that the ratio between the number of poles of rotor to stator (i.e. $\frac{p}{q}$) can be even or odd or fraction. Therefore, this analysis is carried out further for these situations.

3.1.1. Case-I (p/q is even)

The flux developed by the p-pole rotor winding will act like an even harmonic to the q-pole winding of the fictitious machine when it is full-pitched as shown in Figure 3 (second harmonic in this case). Since the even harmonics in the winding function (see Eq. (2)) are absent, the flux linked by each coil will be zero. But this is not true when the q-pole winding is short-pitched. However, the vectorial sum of flux linkages of all coils corresponding to each parallel

path (as $\frac{q}{2}$ parallel paths are available for *q*-pole stator winding of the fictitious machine) will be zero. Analytically, it is confirmed from Eq. (3) (i.e. $\sin\left(\frac{p}{q}\pi\right)$ is zero if *p/q* is even in Eq. (3)). Therefore, *q*-pole winding is perfectly decoupled from the flux developed by the rotor windings of the fictitious machine.

3.1.2. Case-II (p/q is odd)

Since the flux developed by the rotor winding (configured for *p*-poles) is acting like an odd harmonic to the stator winding (configured for *q*-poles) of the fictitious machine, corresponding odd harmonic (i.e. $h=\frac{p}{q}$) of the stator winding can interact with the rotor flux of the fictitious machine. Analytical expressions for this situation can be derived from Eq. (3) as follows:

$$\psi_{qspr}(m_x)=\frac{4gk_{wh}\pi}{pq}\sum_{n=0}^{\frac{q}{2}-1}(-1)^n\cos\left(\frac{p\theta_r}{2}-\frac{2\pi h(m_x-1)}{m}-\frac{\pi p(2n-1)}{q}\right) \tag{4}$$

From Eq. (4), if the number of phases of the *q*-pole stator winding is equal to pole's ratio of rotor to stator of the fictitious machine (i.e. $m=\frac{p}{q}$), flux linked by all phases of the *q*-pole stator windings are exactly equal. It means, the phase voltages induced on the stator windings of the fictitious machine are in same phase with equal magnitude. Therefore, the line voltage seen from the stator side of the fictitious machine is zero. However, if the number of phases of the stator winding (configured for *q*-poles) of the fictitious machine is not equal to the poles ratio of the rotor to the stator of the fictitious machine (i.e. $m\neq\frac{p}{q}$), flux linked by all phases of the *q*-pole stator winding is $\frac{2\pi}{m}$ rad apart from each other with equal magnitude. Hence, the voltages induced on the stator windings are balanced in nature, which results in a strong magnetic coupling between rotor to stator windings even though they are configured for different pole pairs.

3.1.3. Case-III (p/q is a fraction)

From Eq. (3), it may be apparent that the flux-linkage of *q*-pole stator winding (due to the excitation from *p*-pole rotor winding) is not zero, in this case. However, flux linkages (as well as voltages induced) of each parallel path are exactly $\left(\frac{p2\pi}{q}\right)$ rad apart. Hence, these paths cannot be connected in parallel resulting in large circulating currents. However, these paths can be connected in series (since the summation of these parallel path voltages is zero) while developing the individual phases of the stator winding to achieve the magnetic decoupling nature between the windings of the fictitious machine.

3.2. Effect of core saturation

Flux developed by the rotor windings (configured for *p*-poles) of the fictitious machine may saturate due to non-linear B-H characteristics of core material when it is excited. Therefore, odd-order (especially third and fifth harmonics) space harmonics corresponding to the *p*-pole will become significant, and they are equivalent to the formation of 3*p* and 5*p* poles in the airgap. These space harmonics (i.e. 3*p* and 5*p* poles) can interact with the stator winding (configured for *q*-poles) of the fictitious machine when the ratio of rotor to stator poles (i.e. $\frac{p}{q}$) is $\frac{1}{(2n-1)}$ resulting in strong magnetic coupling between the stator and rotor windings of the fictitious machine.

For example, if rotor winding is configured for two poles and overexcited, odd-order space harmonics will become significant. These space harmonics are equivalent to the formation of six (i.e. 3 × 2) poles in the airgap. If the stator winding of the fictitious machine is configured for the six poles, this winding will interact with the space harmonics of the rotor flux causing strong magnetic coupling between them.

Apart from that, the effect of the saturation when both stator and rotor windings (of fictitious machine) are excited at same time is an important aspect that needs to be studied. When both stator (configured for *q*-pole pairs) and rotor (configured for *p*-pole pairs) windings of the fictitious machine are excited, poles which are developed in the airgap due to the excitation will rotate with their respective synchronous speeds. Due to mismatch of the synchronous speeds of these two poles, the phase difference between these two poles will change from

zero to 2π rad. Therefore, total airgap Magneto Motive Force (MMF) (which is the sum of the stator [configured for *p* poles] and rotor [configured for *p* poles] MMFs) can be expressed as

$$F_{total} = F_{qm}\sin\left(\frac{q}{2}\theta_r\right) + F_{pm}\sin\left(\frac{p}{2}\theta_r + \theta_{dsp}\right) \tag{5}$$

F_{qm} and F_{pm} are the peaks of *q* and *p* pole MMFs, respectively. F_{total} is the total MMF in the airgap. θ_r and θ_{dsp} are the angular displacement and phase angle displacement between rotor to stator MMFs of fictitious machine, respectively. Figure 4 shows the total MMF of the fictitious machine for different phase angle displacements (i.e. θ_{dsp} varying from 0 to 2π rads) corresponding to different pole ratios (i.e. *p*/*q* is even [see Figure 4a], odd [see Figure 4b] and fraction [see Figure 4c]). Note that *p*/*q* equal to 8/4, 6/2 and 6/4 pole configurations are considered in the analysis for different pole ratios (i.e. even, odd and fraction, respectively). From these plots, it has been clearly understood that two, two and four peaks will appear for different pole ratios (i.e. even, odd, and fraction) as marked in Figure 4, respectively. The total MMF (i.e. F_{total}) of the fictitious machine feed to the B–H curve and individual flux densities are filtered using a bandpass filter as shown in Figure 5. These peaks will be saturated due to the non-linear B-H characteristics of the core material, and reflect as a two, two and four ripples in the flux density plots for different pole configurations. It means the strength of both rotor and stator poles (of the fictitious machine) will change as one pole is moving on the other. Thus, these ripples in the flux densities will reflect as a sub-harmonic in the induced voltages. The summary of the magnetic decoupling principle is tabulated in Table 1.

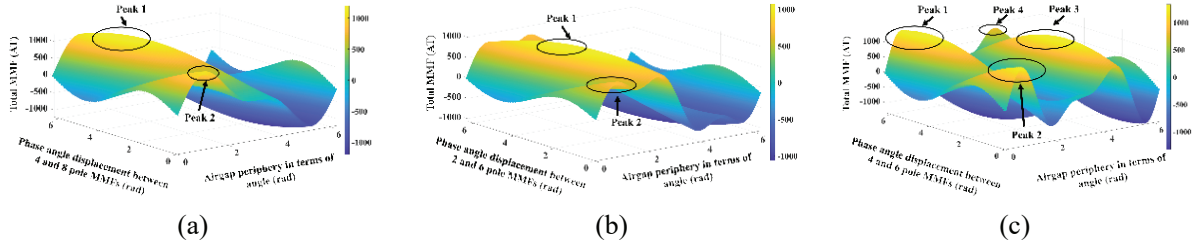

Figure 4. Total MMF of the fictitious machine over the airgap periphery for different phase angle displacements (a) for $\boldsymbol{p/q}$ is even (for example $\boldsymbol{q} = 2$, $\boldsymbol{p} = 4$ and $\boldsymbol{F_{2m}} = 800$, $\boldsymbol{F_{4m}} = 400$) (b) for $\boldsymbol{p/q}$ is odd (for example $\boldsymbol{q} = 2$, $\boldsymbol{p} = 6$ and $\boldsymbol{F_{2m}} = 800$, $\boldsymbol{F_{6m}} = 266.6$) (c) for $\boldsymbol{p/q}$ is fraction (for example $\boldsymbol{q} = 4$, $\boldsymbol{p} = 6$ and $\boldsymbol{F_{4m}} = 800$, $\boldsymbol{F_{6m}} = 533.3$).

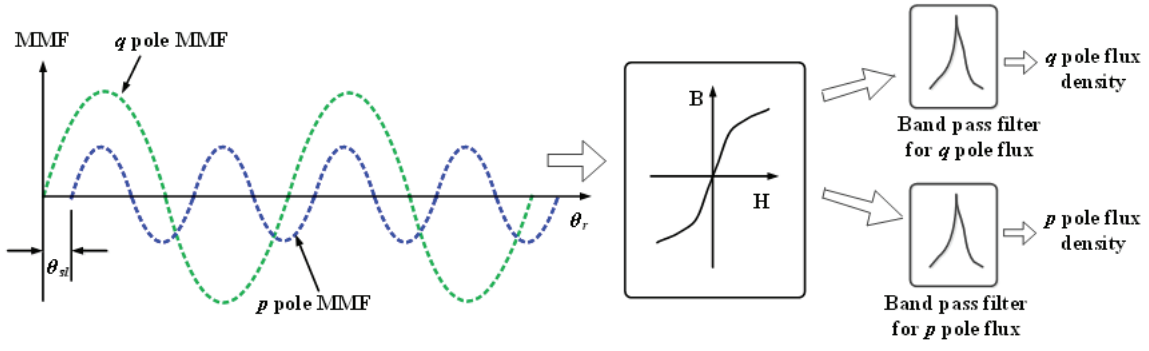

Figure 5. Effect of saturation on individual flux densities when both stator and rotor windings of fictitious machine excited with its rated currents.

Table 1. Effect of *p* pole flux on *q* pole winding of the fictitious machine: a summary

	p/*q* is even	*p*/*q* is odd	*p*/*q* is fraction
$m = p/q$	Decoupled	Zero sequence voltages will be induced in all phases	Not possible
$m \neq p/q$	Decoupled	Coupled	Decoupled
Effect of saturation	Present	Present	Present if *p*/*q* is $1/(2n-1)$
No. of parallel paths	$= q$	$= q$	$\leq q$

4. Machines Developed Using Magnetic Decoupling Theory

Using this magnetic decoupling theory, it can be possible to embed two or more machines which have the same magnetic circuit in the single machine frame. Two new brushless and magnetless SMs, named as Brushless Induction Excited Synchronous Generator (BINSYG), have been proposed by Chakraborty and Rao (2019) and Mondal and Basak (2024).

BINSYG is basically a SM where an IM is inserted in the same magnetic circuit to achieve brushless excitation. SM and IM are configured for different pole pairs to achieve the magnetic decoupling nature. The basic system configuration of the BINSYG is illustrated in Figure 7. It has two sets of three-phase distributed windings on the stator configured for p and q poles, respectively. Similarly, the rotor has a three-phase distributed winding (configured for p poles), and a concentric field winding (configured for q poles). Set of windings configured for p number of poles will act like an IM. Whereas the other set (which is configured for q number of poles) will serve the purpose of SM. A rotating diode bridge rectifier (which is mounted on the rotor structure of the BINSYG as shown in Figure 7) will rectify the induced voltage on the rotor windings of the IM and fed to the field windings of the SM. A controlled inverter placed at the stator side of the IM (see Figure 7) will be used to control the excitation of the SM by entering the different modes of the IM (i.e. generating, motoring and plugging modes). A detailed analysis of design and control of BINSYG is done by Chakraborty and Rao (2019) and Mondal and Basak (2024).

5. Simulation Results

To validate the analysed findings corresponding to the magnetic decoupling principle, BINSYG has been designed for the different pole ratios such as 8/4 pole (i.e. pole ratio is even), 6/2 pole (i.e. pole ratio is odd), and 6/4 pole (i.e. pole ratio is fraction) in the Maxwell-2D platform. Note that IM and SM are configured for 8 and 4 poles, respectively in 8/4 pole BINSYG. Ratings of the above machines are provided in Table 2. The following sub-sections illustrate the simulation results in the practical scenarios discussed in Section 3.

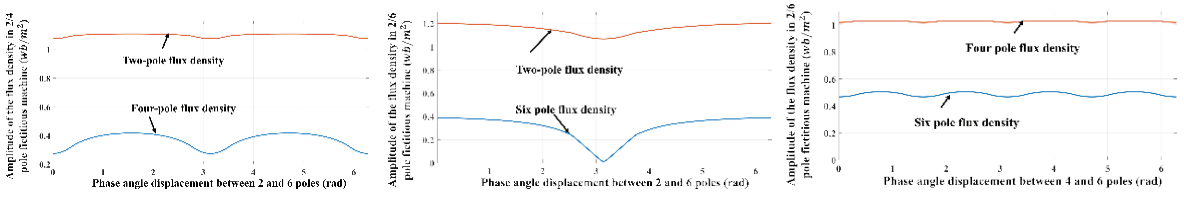

Figure 6. Effect of saturation on the individual flux-densities of fictitious machine when it is configured for (a) p/q is even (for example $q = 2$, $p = 4$) (b) p/q is odd (for example $q = 2$, $p = 6$) (c) p/q is fraction (for example $q = 4$, $p = 6$).

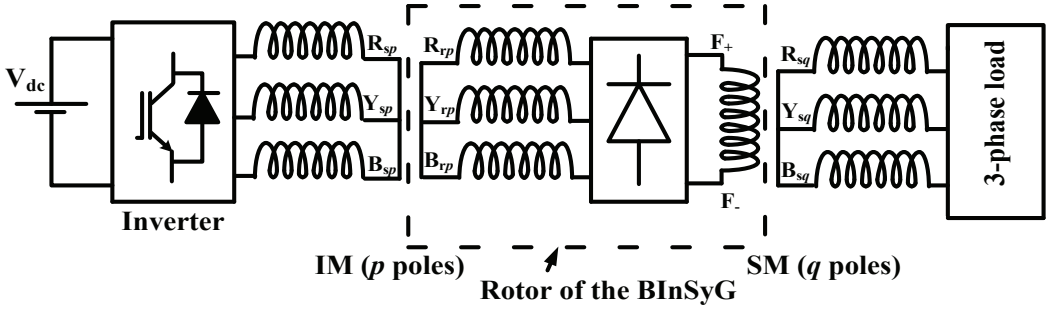

Figure 7. System configuration of the proposed BINSYG. BINSYG, Brushless Induction excited Synchronous Generator; IM, induction machine; SM, synchronous machine.

5.1. Non-sinusoidal winding distribution

5.1.1. Case-I (p/q (i.e. 8/4) is even)

IM configured for eight poles is excited with its rated voltage of 132 V at 50 Hz. Therefore, the IM poles will rotate at a synchronous speed of 750 rpm. Since the rotor is in standstill state, the coils placed on the rotor of the BINSYG will be influenced by these rotating poles. Figure 8a illustrates the voltage induced on the stator coil of the SM (configured for four poles) when it is full-pitched. As analysed in Section 3, flux developed by the IM (constructed for eight poles) will act like an even (second harmonic in this case) harmonic to the full-pitched coil of the SM. Therefore, the voltage induced on this full-pitched coil of SM is exactly zero. However, if the coils of the stator winding of the SM are short-pitched, voltage will be induced on each coil of SM as demonstrated in Figure 8b. Whereas the phase voltage of the stator winding of the SM is the vectorial sum of all the coils corresponding to that phase is exactly zero as presented in Figure 8c. Similarly, voltage induced (which is nullified) on the field winding of the SM is also demonstrated in Figure 8d due to the presence of IM flux. From these simulation results, it can be understood that the SM windings (configured for four pole) are decoupled from flux developed by the IM (configured for eight pole).

5.1.2. Case-II (p/q (i.e. 6/2) is odd)

BINSYG configured for 6/2 pole (i.e. IM and SM are configured for 6 and 2 poles, respectively) is used for the simulation in this scenario. Stator voltage of the IM is excited with the rated voltage (line to line) of 80 V at 50 Hz as shown in Figure 9a. This results in the formation of six poles in the airgap and rotates at 1,000 rpm. Note that the BINSYG is in standstill state. As discussed earlier, these six poles will act like odd harmonic (i.e. third harmonic in this situation) to the stator windings of the SM (configured for two poles). Since the stator winding function also has odd harmonics (especially third harmonic), responding to the six-pole flux, and induce the voltages in each phase as demonstrated in Figures 9b,d and e. When the number of phases (i.e. m) of the SM is equal to the pole ratio (i.e. p/q), voltages induced on all these phases are the same as shown in Figure 9b. Thus, the line voltage will be cancelled itself as demonstrated in Figure 9c. Whereas when the number of phases of the SM does not match with the pole ratio (i.e. p/q), induced voltages on stator windings (configured for five phases) of the SM are balanced as illustrated in Figure 9e. Similarly, voltage induced on field winding of the SM (configured for single phase) is

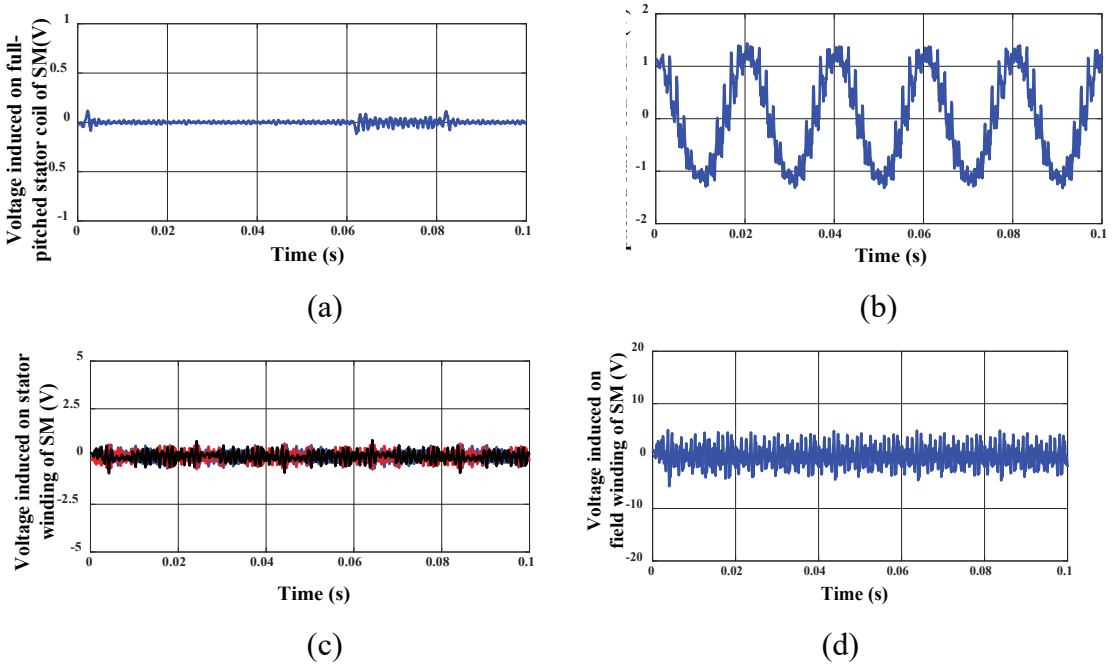

Figure 8. Performance of the magnetic decoupling when p/q (i.e. 8/4) is an even (a) Voltage induced on full pitched stator coil of SM. (b) Voltage induced on short-pitched stator coil of SM. (c) Voltage (phase) induced stator winding of SM. (d) Voltage induced field winding of SM. SM, synchronous machine.

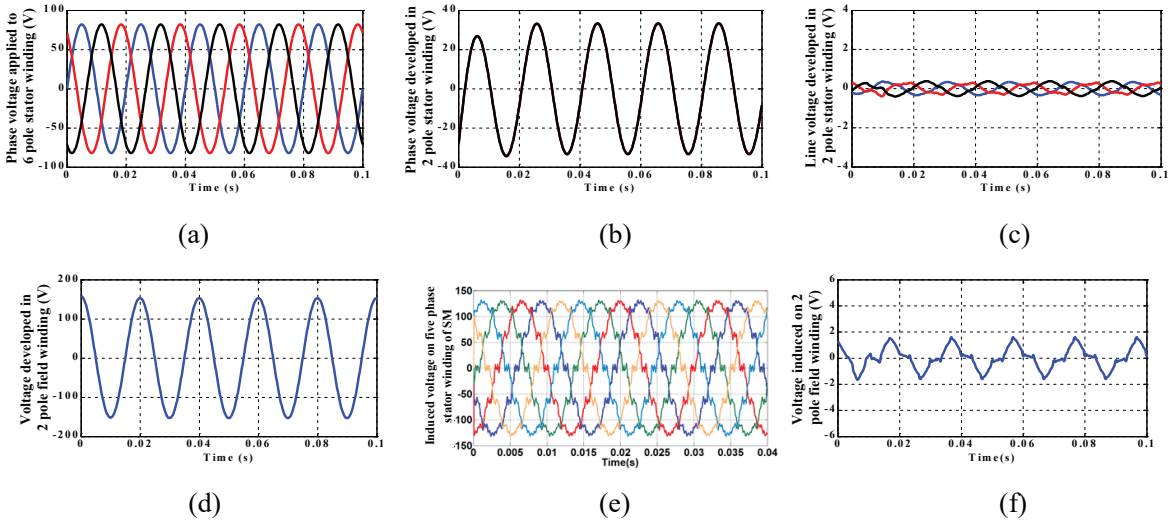

Figure 9. Performance of the magnetic decoupling when p/q (i.e. 6/2) is an odd (a) Voltage applied to stator winding of IM. (b). Induced voltage (phase) on the stator windings of SM ($m = p/q = 3$). (c) Induced voltage (line to line) on stator winding of SM ($m = p/q = 3$). (d) Induced voltage on field winding of SM ($m = 1$ and $p/q = 3$). (e) Induced voltage (phase) on stator winding (constructed for five phases) of SM ($m = 5$ and $p/q = 3$). (f) Induced voltage on field winding (third harmonic is absent on the winding function) of SM ($m = 1$ and $p/q = 3$). IM, induction machine; SM, synchronous machine.

Table 2. Rating and parameters of the BINSYG configured for different pole ratios (i.e. $\frac{p}{q}$ is odd $\left(\frac{p}{q}=\frac{6}{2}\right)$; even $\left(\frac{p}{q}=\frac{8}{4}\right)$ and fraction $\left(\frac{p}{q}=\frac{6}{4}\right)$)

Parameters of the BINSYG	6/2 Pole	8/4 Pole	6/4 Pole
kVA rating of SM/IM (kVA)	3/0.45	5/0.73	5.5/1.1
Voltage rating of SM/IM (V)	250/80	415/132	415/150
Current rating of SM/IM (A)	7/3.2	7.7/3.2	7.7/4.2
Number of poles of SM/IM	2/6	4/8	4/6
Number of stator/rotor slots	45/36	48/36	54/36
Axial core length (mm)	180	210	230
Stator outer diameter (mm)	222.25	260.35	260.35
Stator inner diameter (mm)	139.7	165.5	165.5
Air-gap length (mm)	0.5	0.5	0.5
Rotor outer diameter (mm)	138.7	164.5	164.5
Rotor inner diameter (mm)	41.3	55	55
Flux density of SM/IM $\left(\frac{Wb}{mm^2}\right)$	0.33/0.21	0.39/0.21	0.35/0.2
Specific electric loading of SM/IM (kA/m)	7.5/7.5	7.5/7.5	7.5/7.5
Turns/phase of stator winding of SM/IM	96/72	80/72	90/90
Turns/phase of the rotor winding of SM (filed)/IM	300/24	360/48	320/90

IM, induction machine; SM, synchronous machine.

also demonstrated in Figure 9d which shows the strong magnetic coupling due to the six-pole IM flux. However, to overcome this magnetic coupling, winding function should not have harmonic equal to the pole ratio (i.e. third harmonic in this case). Figure 9f illustrates the induced voltage (almost nullified) on the field winding of the SM whose winding doesn't have the third harmonic.

5.1.3. Case-III (p/q (i.e. 6/4) is fraction)

In this scenario, the stator winding of the IM (configured for six poles) is excited with its rated voltage of 150 V at 50 Hz. Note that the rotor is in standstill state. Figure 10a shows the induced voltages on each parallel path (corresponding to phase A) of the stator winding of SM (configured for four poles). As discussed in Section 3, these parallel path (two parallel paths) voltages are exactly opposite to each other. Therefore, the sum of these voltages will be nullified (see Figure 10b) when the parallel paths are connected in series while forming phase A. Similarly,

voltages induced on the field winding (which is almost zero) of the SM are also illustrated in Figure 10c. From the above results, it can be concluded that the four-pole SM windings are decoupled from the six-pole IM flux.

5.2. Effect of core saturation

As explained in Section 3, the effect of the saturation is more prominent if p/q is $\frac{1}{2n-1}$ (where n is an integer). To understand this phenomenon through simulations, the field winding of the SM corresponding to 6/2 pole BINSYG (where IM and SM are configured for 6 and 2 poles, respectively) is excited with 0.65 A. The prime mover is rotating at 3,000 rpm. Note that this excitation current is in the linear zone of the open circuit characteristics (OCC) as shown in Figure 11. The harmonic spectrum of the voltage induced on the stator windings of the SM (configured for two poles) is illustrated in Figure 12a where the third harmonic component (which will develop six poles in the airgap) is almost absent. Therefore, the voltage induced on the stator windings of the IM is nearly zero as demonstrated in Figure 12b. However, when the field current of the SM is increased to 1.25 A, the third harmonic component in the induced voltage of the SM is significant as shown in Figure 12c. This causes the formation of six poles in the airgap and can interact with the windings of the IM configured for six poles as illustrated in Figure 12d.

As discussed in Section 3, the effect of the core saturation is more prominent when both IM and SM of BINSYG are excited simultaneously. Figure 13 illustrates the consequence of the core with 2.75 A (i.e. rated field current of the SM) and 2.9 A (i.e. rated stator current of the IM) at 30 Hz (f_{im}), respectively. Note that the prime mover is rotating (in the same direction as the IM poles are rotating) at 1,500 rpm which induces voltage at stator terminals of the SM at 50 Hz (f_{sm}). As demonstrated in Figure 6, the relative speed between the SM and IM poles would cause ripple (k = 2 ripples/revolution in this case) in the pole strength of the IM. This ripple causes sub-harmonics in induced voltage of the IM. This can be confirmed from the flux-linked by each stator windings of the IM and its Fast Fourier Transform (FFT) pattern as illustrated in Figures 13a and b, respectively. From this FFT, frequency of the dominant sub-harmonic is 170 Hz (i.e. $k \times f_{sm} \times \frac{P_{im}}{P_{sm}} \pm f_{im}$, $-ve$ sign is for the poles of both SM and IM rotating in

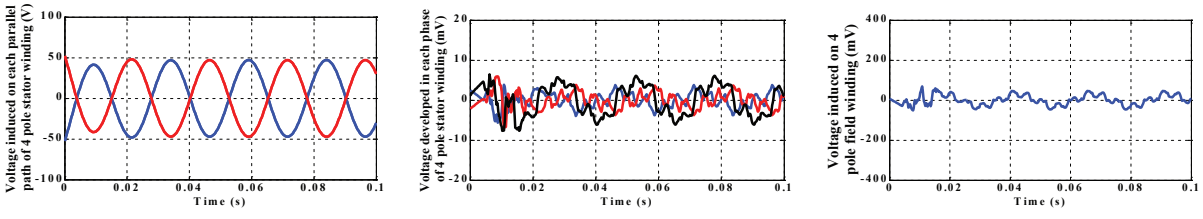

Figure 10. Performance of the magnetic decoupling when $\boldsymbol{p/q}$ (i.e. 6/4) is a fraction. (a). Voltage developed in each parallel path (of phase A) of four pole stator winding. (b). Voltage induced on each phase of four pole stator winding. (c). Voltage induced on field winding of the four pole winding when the six pole stator winding is excited with balanced three-phase supply of 200 V (line to line) at 50 Hz (speed of the rotor is zero and p/q = 3/2).

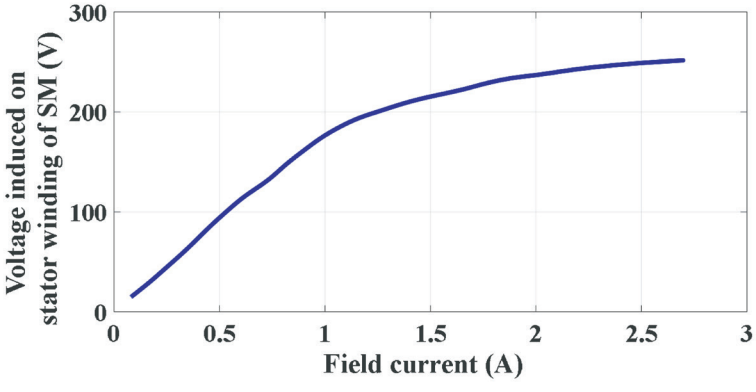

Figure 11. OCC of SM when its field winding is excited (for 2/6 pole BINSYG). OCC, open circuit characteristics; SM, synchronous machine.

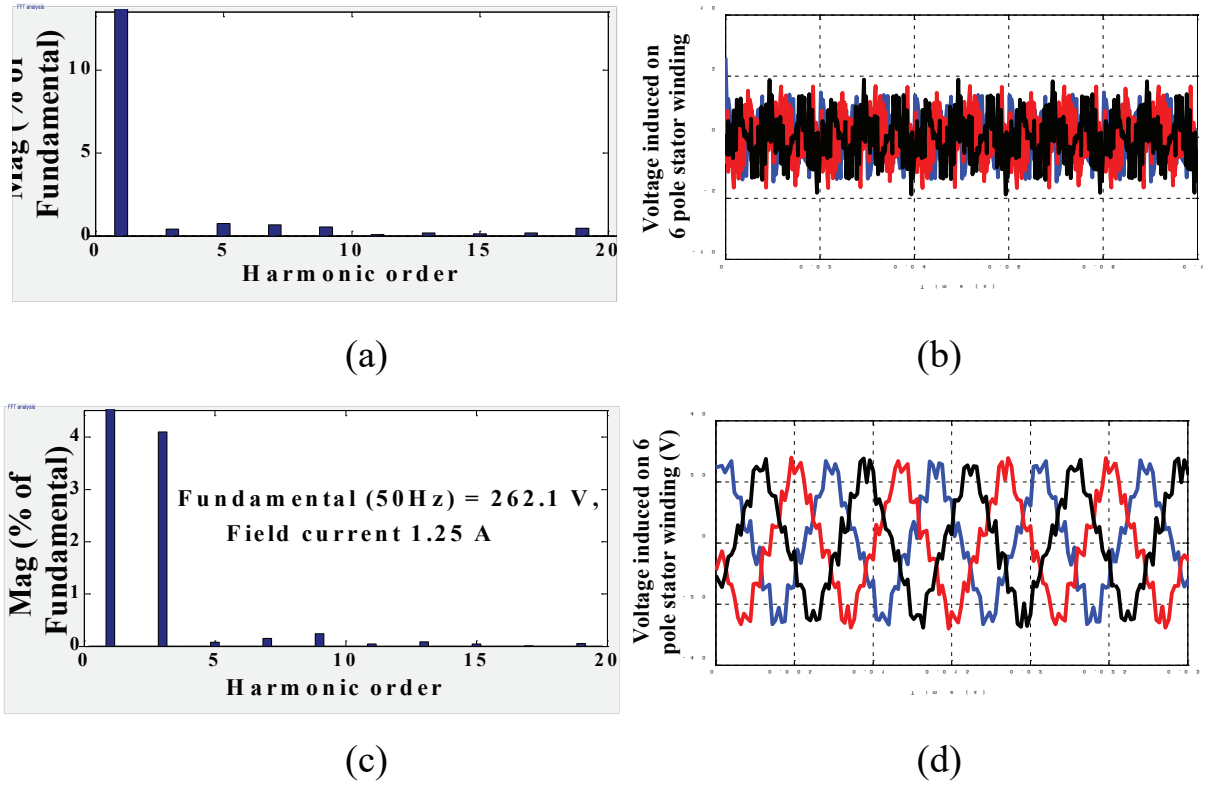

Figure 12. Effect of core (B-H characteristics) saturation on 6/2 pole BINSYG (a). FFT pattern of voltage induced on two pole stator winding when field current is 0.65 A (b). Voltage induced on six pole stator winding when the field winding excited with 0.65 A (speed is 3,000 rpm). (c). FFT pattern of voltage induced on two pole stator winding when field current is 1.25 A. (d). Voltage induced on six pole stator winding when field winding is excited with 1.25 A (speed is 3,000 rpm).

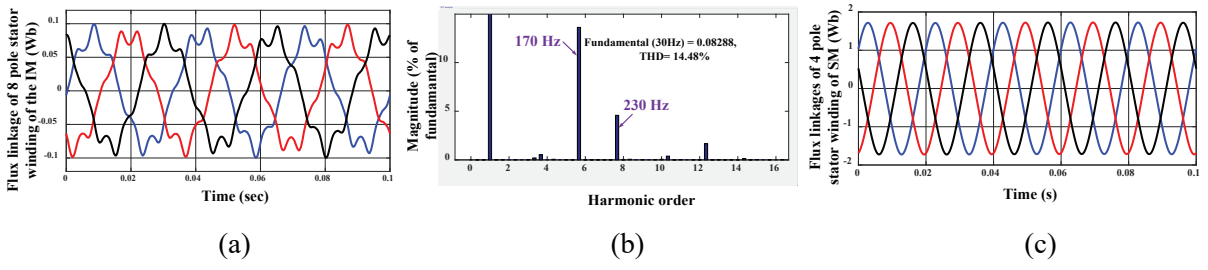

Figure 13. Effect of core saturation on 8/4 pole BINSYG when both field winding of SM and stator winding of IM are excited with 2.75 A and 2.9 A (at 30 Hz), respectively (a). Flux linkage of eight stator winding of IM. (b) FFT of eight pole stator winding of IM. (c). Flux linkage of four pole stator winding of SM. IM, induction machine; SM, synchronous machine.

the same direction, and vice versa) and P_{im} (i.e. eight in this case) and P_{sm} (i.e. four in this case) denote the number of poles of IM and SM, respectively. Figure 13c shows flux linked by the stator winding of SM (configured for four poles) which is harmonic free as expected from the analysis performed in Section 3.

Similar simulations have been conducted on 6/4 pole BINSYG by exciting the field winding of the SM (configured for 6 poles) and stator winding of IM (configured for 6 poles) with 2.5 A and 2.9 A (at f_{im} = 25 Hz), respectively. Note that the prime mover is rotating opposite to the synchronous speed of the IM at 1,500 rpm (f_{sm} = 50 Hz). Figures 14a and b demonstrate the flux linked by the stator windings of IM and its FFT pattern, respectively. From this plot, it has been found that 325 Hz (i.e. $k \times f_{sm} \times \frac{P_{im}}{P_{sm}} + f_{im}$, where k is four as shown in Figure 6c) harmonic is dominant. However, flux-linked (therefore voltage induced) on the stator windings of the SM is harmonic free as demonstrated in Figure 14c.

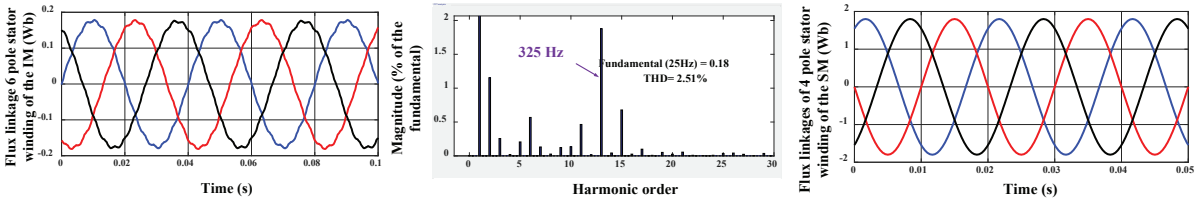

Figure 14. Effect of core saturation on 6/4 pole BINSYG when both field winding of SM and stator winding of IM are excited with 2.5 A and 2.9 A, respectively (a). Flux linkage of six stator winding of IM. (b) FFT of six pole stator winding of IM. (c). Flux linkage of four pole stator winding oof SM. IM, induction machine; SM, synchronous machine.

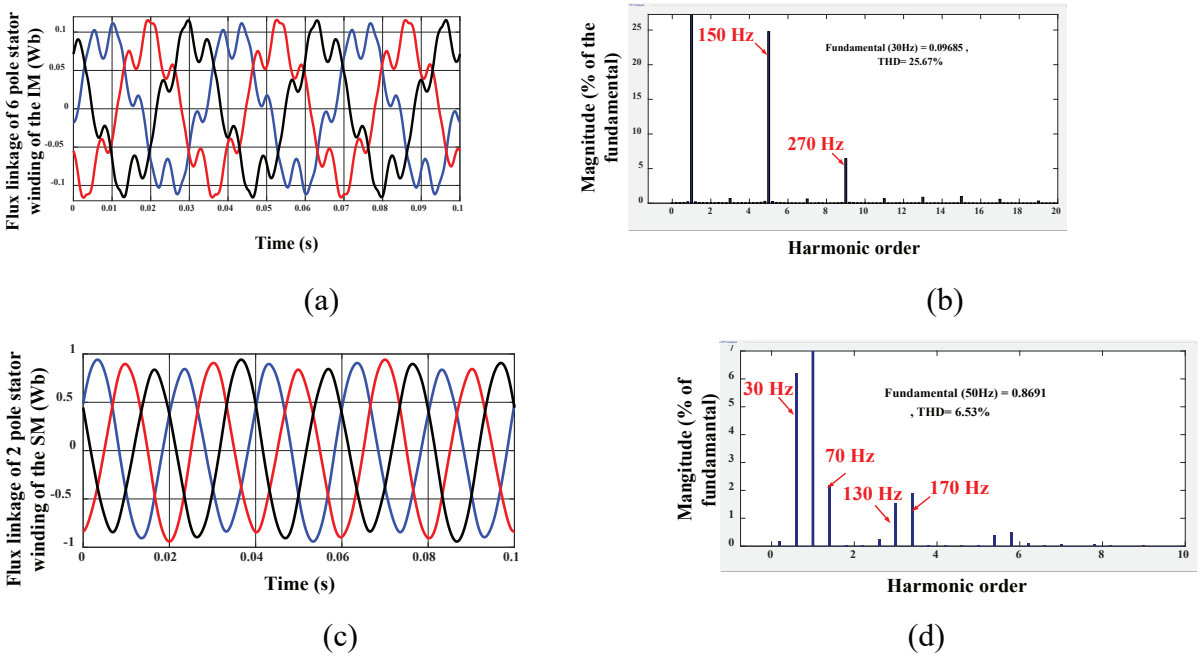

Figure 15. Effect of core saturation on 6/2 pole BINSYG when both field winding of SM and stator winding of IM are excited with 2.5 A and 2.9 A (at 30 Hz), respectively (a). Flux linked by the stator windings of IM (fabricated for six poles). (b) FFT pattern of flux-linked by the stator winding of IM (c). Flux linked by the stator winding of SM (configured for two poles). (d) FFT pattern of flux-linked by the stator windings of the SM. IM, induction machine; SM, synchronous machine.

Figure 15 illustrates the effect of the core saturation when both stator winding of IM (configured for six poles) and field winding of SM (constructed for two poles) of the 6/2 (i.e. pole ratio (p/q) is odd) pole BINSYG are excited with 2.9 A (at f_{im} = 30 Hz) and 2.5 A, respectively. Prime mover is rotating same as the synchronous speed of IM at 3,000 rpm (i.e. f_{sm} = 50 Hz). Figures 15a and b illustrates the flux linked by the stator windings of the IM (constructed for six poles) and its FFT pattern, respectively. As discussed earlier, during the saturation of the two-pole flux (corresponding to SM), third space harmonic will be significant and it is equivalent to the formation of six poles in the airgap. These six poles can interact with the stator windings of the IM and induce 150 Hz (corresponding to 3,000 rpm) component as shown in Figure 15b. Apart from that, due to change in the pole strength of IM while SM poles moving on them, 270 Hz (i.e. $k \times f_{sm} \times \frac{P_{im}}{P_{sm}} + f_{im}$, where k is two) harmonic is becoming dominant as demonstrated in Figure 15b. Similarly, flux linked by the stator winding of the SM and its FFT pattern are shown in Figures 15c and d respectively. Due to the change in the pole strength of the SM (configured for two poles) as shown in Figure 6b, harmonic (i.e. $k \times f_{im} \times \frac{P_{sm}}{P_{im}} + f_{sm}$) flux linkages are induced as shown in Figure 15d. Flux density patterns of the BINSYG configured for different pole ratios are shown in Figure 16.

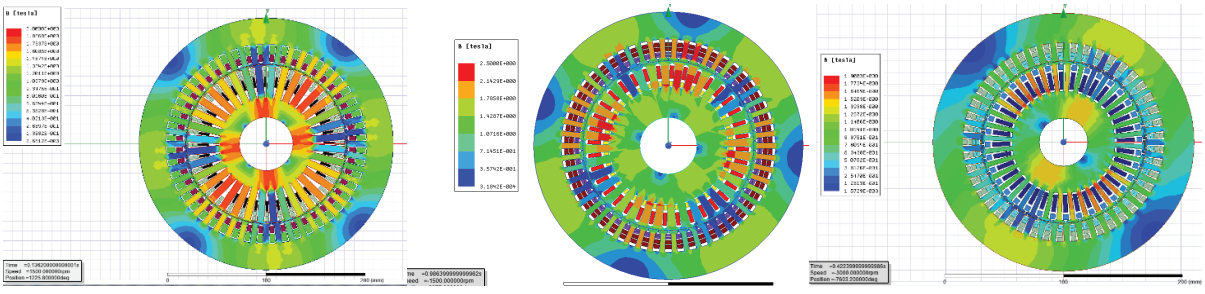

(a) (b) (c)

Figure 16. Flux-density pattern on (a) 8/4 pole (b) 6/4 pole and (c) 6/2 pole BINSYG.

From the above simulation results, it is recommended to choose the number of poles so that p/q is fraction. Apart from this, p/q equal to $1/(2n\text{-}1)$ should be avoided to overcome the effect of core saturation.

6. Experimental Results

Two brushless induction excited synchronous generators (BINSYG) have been developed to verify the simulation results experimentally. In this, one is configured for a 6/2 (IM pole/SM pole) pole combination whereas the other is for 6/4 pole. The experimental machine (designed for 6/4 pole) is illustrated in Figure 17. Note that five slip-rings have been used to bring all the rotor terminals of these machines to stator side to observe the quality of voltage/current waveforms of rotor windings. A diode bridge rectifier is connected externally between the field winding of SM and the rotor winding of IM.

6.1. Case-I (p/q (i.e. 6/2) is odd)

A 6/2 pole (IM poles/SM poles) BINSYG is utilised to understand the magnetic interaction between windings experimentally in this case. The stator winding of the IM (fabricated for six-poles) is excited with 80 V (at 50 Hz) as shown in CH1 of Figure 18a. BINSYG is in standstill state, and the induced voltage on the rotor windings of IM is at 50 Hz as displayed in CH2 of Figure 18a. The voltages induced by the stator winding of SM (designed for two poles) are illustrated in Figure 18b. Since the flux developed by the IM will act like a third harmonic to the SM, voltage induced in all phases (i.e. phase voltage) are in the same phase with magnitude equal as discussed in Section 3. Therefore, they will cancel themselves at line-to-line ends (i.e. line voltage is zero) as illustrated in Figure 18c. Hence, even though SM windings are coupled with the flux developed by the IM at phase voltage level, they cancel themselves at the line voltage level. The induced voltage in the field winding of the SM (<2 V) is presented in Figure 18d. Note that the winding function of the field winding doesn't have the third harmonics.

6.2. Case-II (p/q (i.e. 6/4) is fraction)

BINSYG which is designed for 6/4 (IM poles/SM poles) pole has been used to understand the magnetic decoupling nature in this case. At first, excitation winding (placed on rotor) of SM is energised with the rated current 2.5 A as shown in Figures 19a,b. The speed of the prime mover is maintained at 1,500 rpm. Induced voltage (line to line) on stator winding of SM (configured for four poles) is presented in Figure 19a, and its Root mean square (RMS) value was found to be 632 V. CH2 of Figure 19b displays the voltage (line-to-line) induced on stator winding of IM (configured for six-poles). Its RMS value is <4% of its rated value. Similarly, Figures 19c,d shows the effect of IM (configured for six poles) flux on SM (fabricated for four poles) windings when the stator winding of IM is excited with 220 V (line-to-line). BINSYG is in standstill state which will induce EMF on the rotor coils. Figure 19c illustrates the voltage induced on stator winding of SM (configured for four-poles). It is <1% of its rated. Similarly, voltage induced on field winding of SM is shown in Figure 19d with RMS value of 2 V. Thus, both SM and IM winding are decoupled from one other though configured on the same core material.

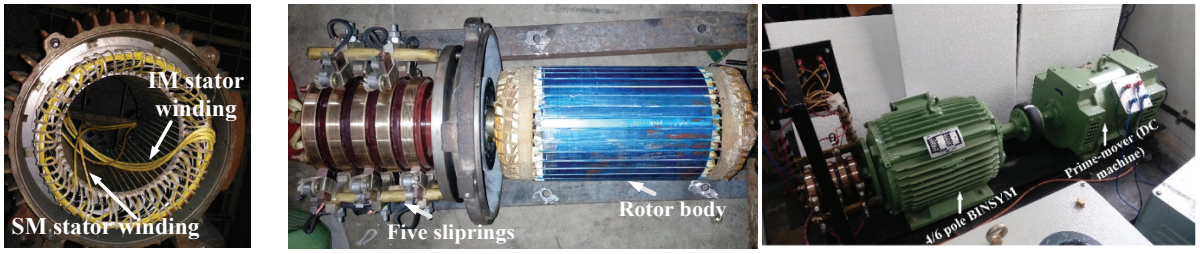

(a) (b) (c)

Figure 17. Experimental prototype of 6/4 pole BINSYG (a) Stator (b) Rotor (c) 6/4 pole BINSYG with DC machine as a prime mover.

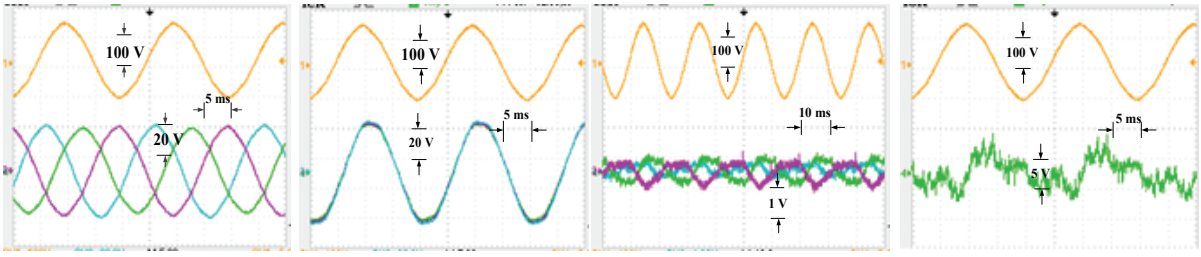

(a) (b) (c) (d)

Figure 18. Effect of IM flux on SM windings for 6/2 pole BINSYG. (a). Voltage (line to line) applied at the stator winding of IM (Yellow) and corresponding voltage induced (blue, pink and green) on rotor windings of IM. (b). Voltage (phase) induced (blue, pink and green) on stator winding of SM. (c). Induced voltage (blue, pink and green) on stator windings of SM. (d) Induced voltage (green) on field winding of SM with winding distribution function not having third harmonic. IM, induction machine; SM, synchronous machine.

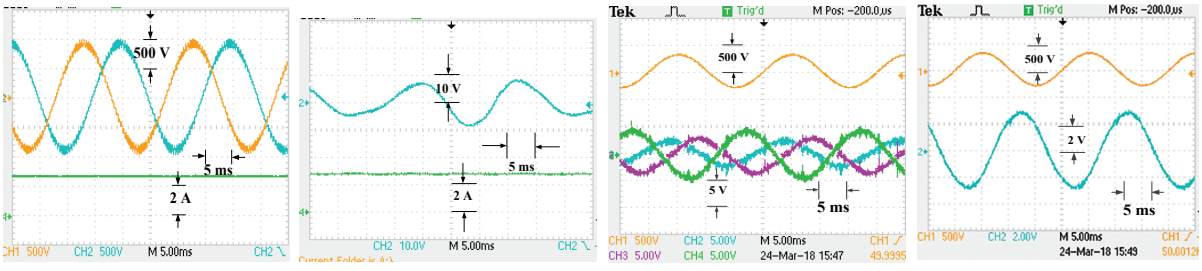

(a) (b) (c) (d)

Figure 19. Effect of SM (configured for four poles) flux on IM (fabricated for six poles) windings and vice versa. (a) Induced voltage (yellow and blue) on the stator windings (line-to-line) of SM. (b) induced voltage (line to line) on stator winding (blue) of IM when the field winding of SM is excited with 2.6 A (green) (speed of the prime-mover is 1,500 rpm). (c) Induced voltage on the stator windings of SM (CH2, CH3 and CH4). (d) Induced voltage on field winding (CH2) of SM when IM stator winding is excited with 220 V (CH1). IM, induction machine; SM, synchronous machine.

6.3. Effect of core saturation (If p/q is 1/(2*n*−1))

In this case, (6/2 pole BINSYG is used for this study) field winding of SM (fabricated for two-poles) is excited with 0.62 A (Which is at the linear zone of OCC) as presented in Figure 20a. Voltage (line-to-line) induced on the stator winding of IM (constructed for six-poles) is shown in CH1 and CH4 of Figure 20a. Since SM flux is not saturated, the voltage induced on the stator winding of IM (7 V RMS) is almost negligible. However, if the field current is increased to 1.25 A, this voltage is increased to 35 V as illustrated in CH1 of Figure 20b. Because of saturation, the third harmonic (equivalent to the formation of six poles in the airgap) will become considerable in SM flux and act like a fundamental to the stator winding of IM. Hence, the frequency of the voltage induced on the stator winding of IM is 150 Hz.

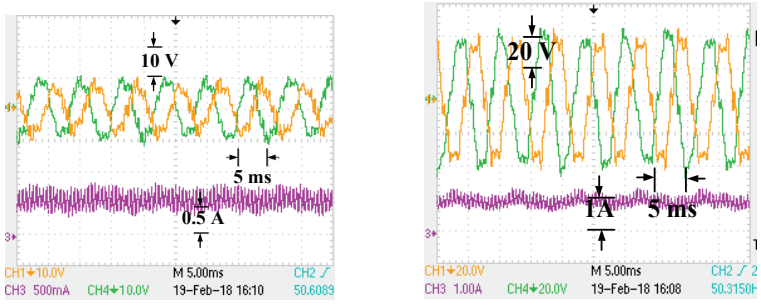

(a) (b)

Figure 20. Effect of SM (configured for two poles) flux on stator winding of IM (fabricated for six poles) (a) Induced line voltage (CH1 and CH4) on stator winding of IM when field winding is excited with 0.62 A (CH3) of current. (b) Induced line voltage (CH1 and CH4) on stator winding of IM when field winding is excited with 1.25 A (CH3) of current. IM, induction machine; SM, synchronous machine.

7. Conclusions

Two or more windings sharing the same magnetic circuit can be magnetically decoupled when configured for different pole pairs. However, to achieve the perfect magnetic decoupling nature, ideal conditions must be met and they are (a) Winding function of the windings must be pure sinusoidal. (b) B-H characteristics of the core material must be linear. (c) Space harmonics in the magnetic field due to the slot openings should be zero. But, in practical scenarios, achieving the above ideal conditions are not possible due to the limited number of slots, core saturation, etc. In this work, a detailed mathematical analysis of simulation and experimental results is reported after considering the practical scenarios for the machines with multiple windings fabricated for different pole pairs. Based on this principle, a new brushless and permanent magnetless machines was developed named brushless induction excited synchronous generator (BINSYG) SM. The basic system configuration of this machines is discussed briefly to understand the architecture of the BINSYG. Experimental results from the laboratory prototypes of BINSYG confirm the findings of mathematical analysis and simulation results.

References

Ademi, S., Jovanović, M. G. and Hasan, M. (June 2015). Control of Brushless Doubly-Fed Reluctance Generators for Wind Energy Conversion Systems. *IEEE Transactions on Energy Conversion*, 30(2), pp. 596–604.

Ali, Q., Lipo, T. A. and Kwon, B. I. (Nov 2015). Design and Analysis of a Novel Brushless Wound Rotor Synchronous Machine. *IEEE Transactions on Magnetics*, 51(11), pp. 1–4.

Ayub, M., Hussain, A., Jawad, G. and Kwon, B.-I. (June 2019). Brushless Operation of a Wound-Field Synchronous Machine Using a Novel Winding Scheme. *IEEE Transactions on Magnetics*, 55(6), pp. 1–4.

Chakraborty, C. and Rao, Y. T. (Dec 2019). Performance of Brushless Induction Excited Synchronous Generator. *IEEE Journal of Emerging and Selected Topics in Power Electronics*, 7(4), pp. 2571–2582.

Cingoski, V., Mikami, M., Yamashita, H. and Inoue, K. (May 1999). Computer Simulation of A Three-Phase Brushless Self-Excited Synchronous Generator. IEEE *Transactions on Magnetics*, 35(3), pp. 1251–1254.

Dhaouadi, R., Kubo, K. and Tobise, M. (Sep/Oct 1993). Two-Degree-of-Freedom Robust Speed Controller for High-Performance Rolling Mill Drives. *IEEE Transactions on Industry Applications*, 29(5), pp. 919–926.

Griffo, A., Wrobel, R., Mellor, P. H. and Yon, J. M. (Sept–Oct 2013). Design and Characterization of a Three-Phase Brushless Exciter for Aircraft Starter/Generator. *IEEE Transactions on Industry Applications*, 49(5), pp. 2106–2115.

Guerrero, J. M. and Ojo, O. (March 2009). Total Airgap Flux Minimization in Dual Stator Winding Induction Machines. *IEEE Transactions on Power Electronics*, 24(3), pp. 787–795.

Hammad, S. Y., Ikram, J., Badar, R., Bukhari, S. S. H., Khan, L. and Ro, J.-S. (2023). Performance Analysis of Brushless Wound Rotor Vernier Machine by Utilizing Third Harmonic Field Excitation. *IEEE Access*, 11, pp. 65480–65490.

Hussain, A. and Kwon, B.-I. (Sep 2018). A New Brushless Wound Rotor Synchronous Machine Using A Special Stator Winding Arrangement. *Electrical Engineering*, 100(3), pp. 1797–1804.

Inoue, K., Yamashita, H., Nakamae, E. and Fujikawa, T. (Sep 1992). A Brushless Self-Exciting Three-Phase Synchronous Generator Utilizing the 5th-Space Harmonic Component of Magnetomotive Force Through Armature Currents. *IEEE Transactions on Energy Conversion*, 7(3), pp. 517–524.

Jawad, G., Ali, Q., Lipo, T. A. and Kwon, B. I. (July 2016). Novel Brushless Wound Rotor Synchronous Machine with Zero-Sequence Third-Harmonic Field Excitation. *IEEE Transactions on Magnetics*, 52(7), pp. 1–4.

Krause, P. C., Wasynczuk, O. and Sudhoff, S. D. (2013). *Analysis of Electric Machinery and Drive Systems*. Delhi: Wiley-IEEE Press.

Lipo, T. A. (2012). *Analysis of Synchronous Machines*. Delhi: CRC Press.

Liu, H., Yan, Y., Bu, F., Huang, W., Jiang, W., Tan, Y. and Qian, Z. (Feb 2024). Sensor-Less Control with Adaptive Speed Observer Using Power Winding Information for Dual-Stator Winding Induction Starter/Generator. *IEEE Transactions on Industrial Electronics*, 71(2), pp. 1388–1398.

Mondal, A. K., Basak, S. and Chakraborty, C. (2024). Excitation control of Brushless Induction Excited Synchronous Motor (BINSYM) with Induction Machine operating in deep-plugging mode. *Power Electronics and Drives*, 9(44).

Munoz, A. R. and Lipo, T. A. (Sept/Oct 2000). Dual Stator Winding Induction Machine Drive. *IEEE Transactions on Industry Applications*, 36(5), pp. 1369–1379.

Nonaka, S. and Kawaguchi, T. (Nov–Dec 1992). Excitation Scheme of Brushless Self-Excited-Type Three-Phase Synchronous Machine. *IEEE Transactions on Industry Applications*, 28(6), pp. 1322–1329.

Rafin, S. M. S. H. and Mohammed, O. A. (Nov 2023). Novel Dual Inverter Sub-Harmonic Synchronous Machines. *IEEE Transactions on Magnetics*, 59(11), pp. 1–5.

Vaidyaa, J. G., Bansal, M. L. and Mansir, H. (Jun 9, 1998). Multiple Output Decoupled Synchronous Generator and Electrical System Employing Same. United States Patent 5,764,036.

Yao, F., An, Q. and Sun, L. (June 2022). Voltage Stabilization Analysis of a Harmonic Excitation Generator Employing Armature Current Auxiliary Self-Excitation Scheme Under Variable Load Conditions. *IEEE Transactions on Industrial Electronics*, 69(6), pp. 5432–5441.

Yao, F., An, Q., Gao, X., Sun, L. and Lipo, T. A. (Sept–Oct 2015). Principle of Operation and Performance of a Synchronous Machine Employing a New Harmonic Excitation Scheme. *IEEE Transactions on Industry Applications*, 51(5), pp. 3890–3898.

Yao, F., An, Q., Sun, L. and Lipo, T. A. (Nov 2016). Performance Investigation of a Brushless Synchronous Machine with Additional Harmonic Field Windings. *IEEE Transactions on Industrial Electronics*, 63(11), pp. 6756–6766.

Yao, F., Sun, L., Sun, D. and Lipo, T. A. (July–Aug 2021). Design and Excitation Control of a Dual Three-Phase Zero-Sequence Current Starting Scheme for Integrated Starter/Generator. *IEEE Transactions on Industry Applications*, 57(4), pp. 3776–3786.